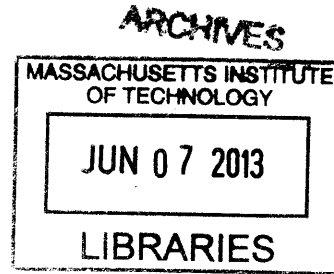


Design of Test Bench Apparatus for Piezoelectric Energy Harvesters

by

You C. Yoon



Submitted to the
Department of Mechanical Engineering
in Partial Fulfillment of the Requirements for the Degree of
Bachelor of Science in Engineering as Recommended by the
Department of Mechanical Engineering

at the

Massachusetts Institute of Technology

June 2012

[June 2013]

© 2012 You C. Yoon. All rights reserved.

The author hereby grants to MIT permission to reproduce and to distribute publicly paper and electronic copies of this thesis document in whole or in part in any medium now known or hereafter created.

Signature of Author: _____
Department of Mechanical Engineering
May 09, 2012

Certified by: _____
Sang-Gook Kim
Professor of Mechanical Engineering
Thesis Supervisor

Accepted by: _____
John H. Lienhard V
Samuel C. Collins Professor of Mechanical Engineering
Undergraduate Officer

Design of Test Bench Apparatus for Piezoelectric Energy Harvesters

by

You C. Yoon

Submitted to the Department of Mechanical Engineering
on May 09, 2012 in Partial Fulfillment of the
Requirements for the Degree of

Bachelor of Science in Engineering as Recommended by the
Department of Mechanical Engineering

ABSTRACT

This thesis presents the design and analysis of an experimental test bench for the characterization of piezoelectric microelectromechanical system (MEMS) energy harvester being developed by the Micro & Nano Systems Laboratory research group at MIT. Piezoelectric MEMS energy harvesters are micro-devices that are able to harvest energy from their ambient vibrations using piezoelectric material property, and many different designs are being researched by the Micro & Nano Systems Laboratory. In order to analyze the different designs, it is crucial to have a flexible test bench, and the test bench created in this thesis allows data to be gathered easily from different energy harvesters. After the test bench is designed and created, it is used to excite a linear cantilever beam energy harvester system at different frequencies and values for open circuit voltage, resonance frequency, and maximum power are calculated from the collected experimental data. In addition, theory behind linear and nonlinear energy harvester systems is investigated and important definitions, characteristics, and equations are summarized in this thesis.

Thesis Supervisor: Sang-Gook Kim
Title: Professor of Mechanical Engineering

Acknowledgements

I would like to thank Professor Sang-Gook Kim and the rest of the Micro & Nano Systems group at MIT Pappalardo Laboratory for giving me the opportunity to work with and learn from them. My research experience at the Micro & Nano Systems group strengthened my understanding of mechanical engineering principles and further enhanced my research abilities. I would also like to give a special thank you to my direct supervisor, Ray Xu, for taking me under his wing. In addition to mentoring my research, he also provided countless hours of guidance for my work in this thesis.

I would also like to thank Stephen Bathurst and Arman Hajati for their supervision and guidance which helped develop my research skills and understanding of mechanical engineering concepts.

Finally, I would like to thank my family for their continual support throughout my education process and beyond.

Table of Contents

Abstract	2
Acknowledgements	3
Table of Contents	4
List of Figures	5
List of Tables	6
1. Introduction	7
1.1 General Idea of MEMS Energy Harvester	7
1.1.1 Electrostatic Energy Harvester	7
1.1.2 Electromagnetic Energy Harvesting	8
1.1.3 Piezoelectric Energy Harvesting	9
1.2 Important Factors Regarding Power Measurement and MEMS Design	9
1.2.1 Linear MEMS System	10
1.2.2 Nonlinear MEMS System	12
1.3 Overview of the Thesis	15
2. Design of the Test System	16
2.1 Overall Layout of the Test System	16
2.2 Details Regarding the Shaker	18
2.3 Details Regarding the Charge Amplifier	18
2.4 Details Regarding the DAQ Board	20
3. Experimental Evaluation	21
3.1 Specification of Energy Harvester Device	21
3.2 Open Circuit Measurements for the Energy Harvester	23
3.3 Theoretical Calculation of Power	28
3.4 Experimental Calculation of Power	30
4. Summary and Conclusion	32
5. Appendices	33
Appendix A LabView Setup	33
Appendix B ET-126 Shaker Specifications	39
Appendix C Charge Amplifier Specifications	41
Appendix D NI USB-6120 DAQ Board Specifications	43
Appendix E V21BL Specifications	47
Bibliography	48

List of Figures

Figure 1-1:	possible topologies for MEMS-scale electrostatic energy harvester	8
Figure 1-2:	mechanical schematic of a typical electromagnetic energy harvester	9
Figure 1-3:	A diagram of a cantilever beam harvester with a proof mass	10
Figure 1-4:	Graph of transmissibility.....	11
Figure 1-5:	Bending and stretching of a double clamped beam.....	13
Figure 1-6:	Deflection vs. frequency for a nonlinear system	14
Figure 2-1:	Diagram of the overall layout of the test bench	16
Figure 2-2:	Test bench layout with labeled machinery	17
Figure 2-3:	Test bench layout with labeled machinery	17
Figure 2-4:	Energy harvester mounted on the shaker	18
Figure 2-5:	Input and output chord of the charge amplifier	19
Figure 2-6:	5000B-100A charge amplifier with a gain of gain of 100mV/pC	19
Figure 3-1:	Diagram of V21BL energy harvester; measurements are in inches	21
Figure 3-2:	Layers of V21BL.	22
Figure 3-3:	Graph that shows the relationship between natural frequency and proof mass.....	22
Figure 3-4:	Positive and negative nodes of the energy harvester connected to clamps	23
Figure 3-5:	Green wire inserted in Input1 and black wire inserted in Ground of the DAQ board	24
Figure 3-6:	Diagram of overall layout of the test bench without charge amplifier.....	24
Figure 3-7:	Open circuit voltage measured at 67Hz.....	25
Figure 3-8:	Plot of open circuit voltage vs. frequency for a V21BL.....	27
Figure 3-9:	Series circuit with voltage source and internal and external impedance	28
Figure 3-10:	Pattern seen from plotting $P_{ext}(Z_{ext})$ function	29
Figure 3-11:	Resistor connecting the positive and negative nodes of energy harvester	30
Figure 3-12:	Graph that plots power vs. resistance data from table 3-2.....	31

List of Tables

TABLE 3-1:	Open circuit voltage created by the energy harvester for given excitation frequency ...	26
TABLE 3-2:	Power values calculated from the resistance swap.....	31

1. Introduction

1.1 General Idea of MEMS Energy Harvester

Many technologies have been developed to collect energy from our ambient surroundings, such as wind turbines, solar panels, and wave turbines. One of the more recent energy harvesting technologies is the idea of MEMS Energy Harvester from passive environmental vibrations. Vibrational MEMS energy harvesting is a fairly new technology that can be categorized into three main methods: electrostatic, electromagnetism, and piezoelectric. Although this thesis focuses on piezoelectric energy harvesters, different types of harvesting method will be briefly discussed for general information.

1.1.1 Electrostatic Energy Harvesting

The main idea behind electrostatic energy harvester comes from the relationship between the capacitance of a capacitor and the distance between the capacitors. As distance between the capacitors increase, the capacitance decreases, which decreases charge; as distance between the capacitors decrease, the capacitance increases, which increases charge. By using this characteristic of a capacitor, charge created from mechanical energy can be used to create electrical energy [1].

The main disadvantage of this energy harvesting method is that the harvester needs a separate voltage source for the capacitors and there also has to be a mechanical motion-limiting mechanism so the electrodes of the capacitors don't create a short circuit. Lack of reliability and complexity of the electrostatic energy harvesting method makes piezoelectric energy harvesting method preferable over the electrostatic method.

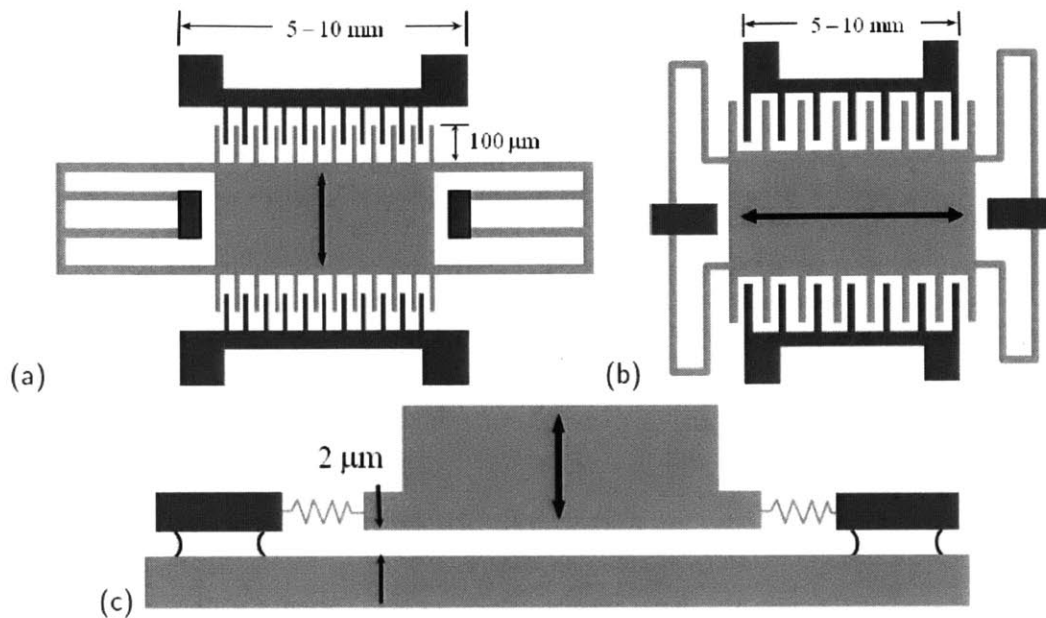


Figure 1-1: Three possible topologies for MEMS-scale electrostatic energy harvester: (a) in-plane overlap type, (b) in-plane gap closing type, (c) out-of-plane gap closing type [2].

1.1.2 Electromagnetic Energy Harvesting

Electromagnetic energy harvester uses a similar mechanism used in large-scale generators. Using a magnet and a coil, Faraday's law of induction is applied by changing the magnetic flux felt by the coil; a permanent magnet is held in place while the coil moves up and down changing the magnetic flux and creating an electric current [3].

Although this method is simple there are three main problems to this energy harvesting method. Firstly, the current density is high but the induced voltage is limited to hundreds of millivolts. Secondly, The EM generator requires a structure that allows big range of movements and it needs a bulky magnetic structure. Thirdly, single fabricating process for induction coils and magnet are not compatible with standard MEMS procedures; they need to be precision machined and assembled, which is very costly. Therefore, the production cost is very high and may not be commercially viable.

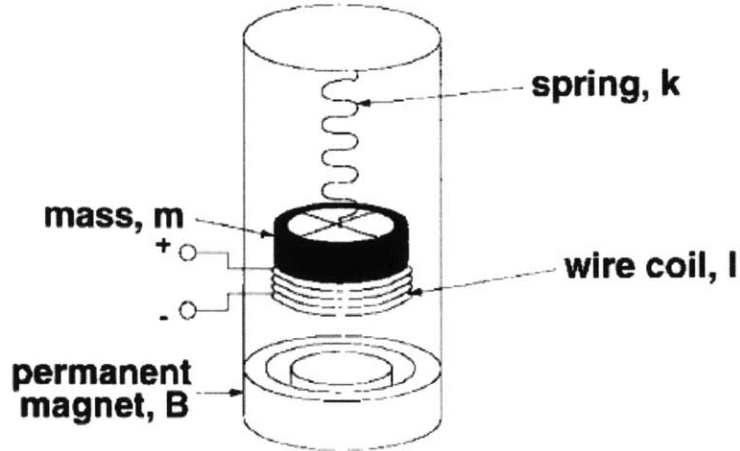


Figure 1-2: The mechanical schematic of a typical electromagnetic energy harvester [3].

1.1.3 Piezoelectric Energy Harvesting

Piezoelectric material's unique property allows energy to be harvested from the material's mechanical strain. When strain is exerted on a piezoelectric material, the molecules of piezoelectric material interact to create electrical charge, and this charge can be harvested to create energy. To exert physical strain on the piezoelectric material, the material can be vibrated, such as vibrating a piezoelectric cantilever beam, and energy can be harvested from the piezoelectric material. MEMS-piezoelectric energy harvesters can have power density up to $3.6\text{W}/\text{cm}^3$ and voltage up to 10V. Piezoelectric energy harvesters' efficient energy generation and simple design structures make them favorable compared to the other two energy-harvesting methods.

1.2 Important Factors Regarding Power Measurement and MEMS Design

The power measurements for the MEMS energy harvester have to be made for low frequencies because the MEMS devices are to be used for practical usage and will be powered by ambient vibrations, which are mostly in low frequencies. Also, since the MEMS device will be operated in low frequency, it is important that the resonance frequency of the device is in the range of ambient vibration. This is important because the charge created by piezoelectric material is directly proportional to the strain put on the material and at resonance frequency the strain exerted on the material is at max. In addition, the frequency range around the resonance

frequency gives high strains, and it's important to have the operating frequency to be around the range of the resonance frequency so energy can be created efficiently. In order to achieve these traits many different designs of MEMS device are being researched and two systems of MEMS systems that will be discussed below are linear and non-linear systems

1.2.1 Linear MEMS System

A simple example of a linear MEMS system is a cantilever beam harvester with a proof mass on the edge of the beam.

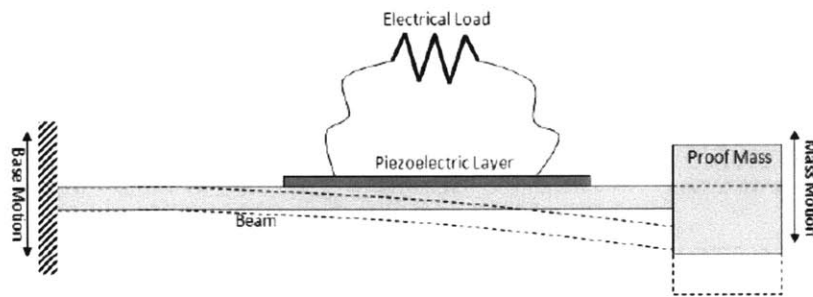


Figure 1-3: A diagram of a cantilever beam harvester with a proof mass; linear system [2].

For this linear system, equation relating force, deflection, and properties of the beam can be derived to calculate the deflection of the beam for a given proof mass and force. Using variable F as the force exerted on the system, which is proof mass multiplied by the acceleration exerted on the system by the vibration, δ as the deflection of the beam, E as the young's modulus, and W as the width, H as the thickness, and L as the length of the beam, the equation derived is [4]:

$$F = \frac{EW H^3}{4L^3} \delta \tag{1-1}$$

In addition, given linear stiffness, K_L , and mass of proof mass, m_{pm} , an equation that calculates the natural frequency is given by the following equation [5]:

$$f_n = \frac{1}{2\pi} \sqrt{\frac{K_L}{m_{pm}}} \tag{1-2}$$

For a MEMS energy harvester, we can plot a transmissibility vs. frequency graph, which is proportional to gain voltage vs. frequency graph, and imply that transmissibility is directly proportional to the deflection, energy, power, and current created by the harvester. For linear MEMS system, such as a cantilever beam, following plots for given damping coefficients display its characteristic.

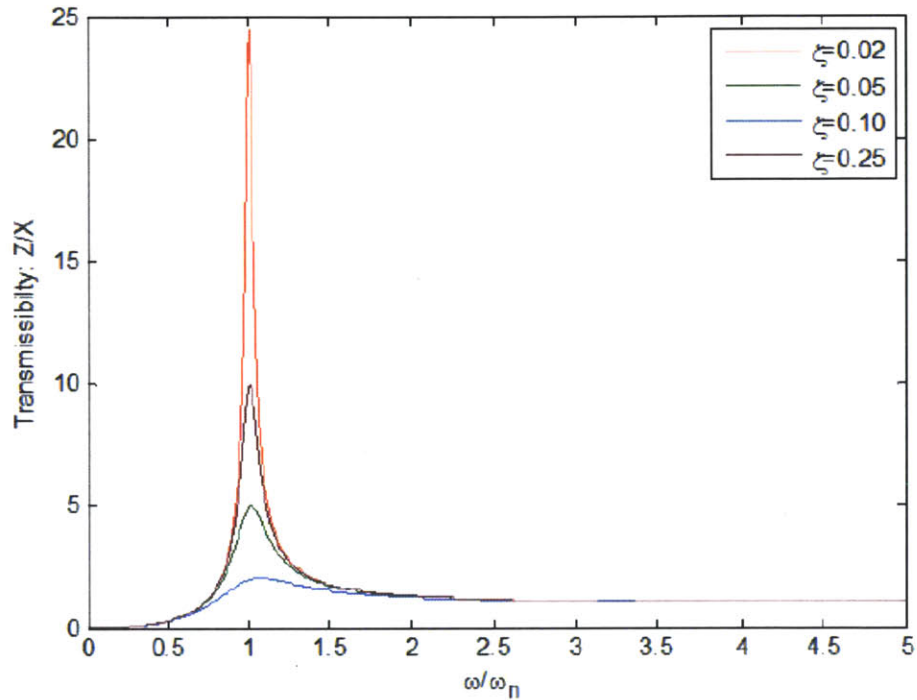


Figure 1-4: Graph of transmissibility, also known as linear gain, vs. normalized frequency for a linear system for given damping values [2].

Damping for MEMS device is a combination of mechanical and electrical damping. Some mechanical damping sources are squeeze film damping, suspension/anchor losses, and thermo-elastic dissipation, while a main electrical damping source is electrical loss from external electrical load. Mechanical damping can't be controlled too much, but electrical damping may be altered in small amount by changing the external electrical load [6].

From looking at the graph above, it can be seen that when there is less damping in the system, there is higher linear gain. One of the most important characteristic for an energy

harvester is the quality factor Q , which tells how much energy a system conserves. Equation for Q is given by [2]:

$$\frac{\Delta\omega}{\omega_n} = \frac{1}{Q} \quad (1-3)$$

Bandwidth, $\Delta\omega$, is the frequency range at half max gain. It's interesting to note that to maximize quality factor, less damping is preferred, which maximizes the gain and lowers bandwidth range. However we also need a wide bandwidth range so our device can function and create energy efficiently in a wide frequency range, and more damping is preferred in this case. So it is crucial to create a design that has high enough Q factor and gain, but also a wide bandwidth. This shows that damping and bandwidth are inversely proportional to gain. However, large bandwidth range and high gain are both preferred, and this is the "Gain-Bandwidth Dilemma" [7].

In addition, as it can be seen from the graph above, some traits of linear systems are narrow bandwidth and sensitivity of transmissibility, voltage, current, and power to the change in frequency. This limits linear systems to a small frequency range in which they can operate efficiently, and this makes linear systems not very viable for real world applications. Another reason why linear systems are not preferred is because the maximum output power of linear systems is limited by the internal impedance of the energy harvester (this idea will be explained in section 3.3). Due to these drawbacks in linear systems, non-linear systems are being researched to develop viable energy harvesters.

1.2.2 Non-linear MEMS System

As seen from section 1.2.1, the bandwidth of a linear system is very narrow, the power created by the system is limited by internal impedance, and power, voltage, current, and transmissibility are very sensitive to the change in frequency. This causes the system to have a very narrow frequency range that it can function efficiently. In order to improve this design, a non-linear system can be introduced. An example of a non-linear device is a double clamped cantilever beam with a proof mass in the middle.

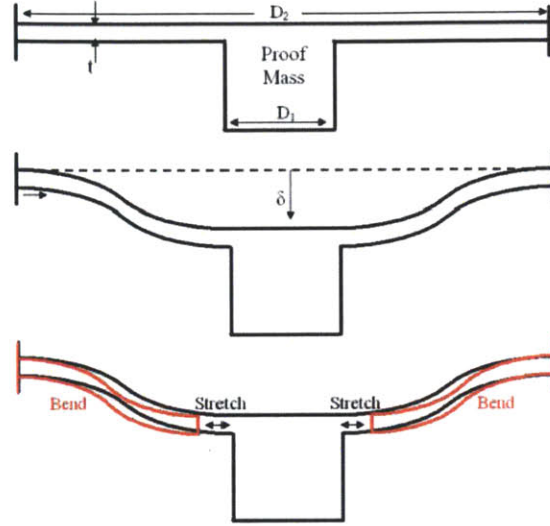


Figure 1-5: Bending and stretching of a double clamped beam; nonlinear system [2].

When the deflection is low the double clamped cantilever beam still behaves like a linear system since there isn't a stretching displacement and a simple equation can be used to calculate its deflection. Using variable F as the force exerted on the system, which is proof mass multiplied by the acceleration exerted on the system by the vibration, δ as the deflection of the beam, E as the young's modulus of the beam, and W as the width, H as the thickness, and L as the length of the beam, the equation derived is [4]:

$$F = \frac{16EWH^3}{L^3} \delta \quad (1-4)$$

When the deflection is high, the double clamped cantilever beam behaves nonlinearly and goes through stretching as well as the vertical displacement. Under this condition, given that σ_0 is residual axial stress and ν is Poisson's ratio, following equation of displacement and force can be derived [8].

$$F = \left\{ \left(\frac{\pi^2}{2} \right) \left(\frac{\sigma_0 W t}{L} \right) + \left(\frac{\pi^4}{6} \right) \left[\frac{E W t^3}{(1-\nu^2) L^3} \right] \right\} \delta + \left(\frac{\pi^4}{8} \right) \left[\frac{E W t}{(1-\nu) L^3} \right] \delta^3 \quad (1-5)$$

In addition, given linear stiffness, K_L , mass of proof mass, m_{pm} , nonlinear stiffness due to stretching, K_S , and maximum displacement, δ , natural frequency can be found using the following equation [2]:

$$f_{n,eq} = \frac{1}{2\pi} \sqrt{\frac{k_L + \frac{3}{4}\delta^2 k_S}{m_{pm}}} \tag{1-6}$$

To study the characteristics and the relationship between frequency and deflection of a nonlinear system, a deflection vs. frequency graph for a nonlinear MEMS system can be plotted as seen below. It is important and interesting to note the different zones of the plot: unstable root, unique root, high-energy stable root, and low-energy stable root, and how previous events are important, as if the nonlinear system has a memory. For example, when frequency is increased from 0 Hz to the frequency value at the dotted light blue line, about 1080Hz, the deflection drops rapidly and will follow the green line when frequency is decreased. At this region, even though the system is excited at the same frequency as before, such as 700 Hz, deflection will not be the same as the value on the solid light blue lines.

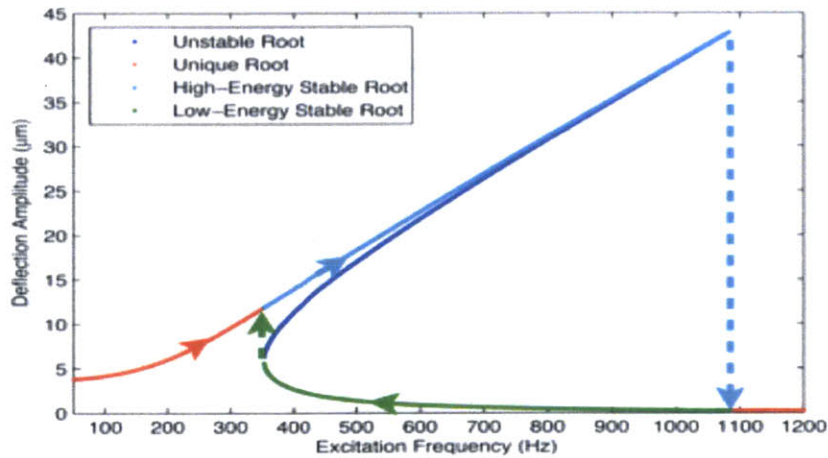


Figure 1-6: Deflection vs. frequency for a nonlinear system. The system has a memory once frequency passes 1080Hz [2].

From looking at the graph above, it can be seen that the nonlinear system has a greater bandwidth range than the linear system. Also, the nonlinear system is less sensitive to frequency change, and change in power, current, and energy due to change in frequency won't be as extreme as that of a linear system. In the plot above, as long as frequency is above 350Hz and under 1080Hz, the system will function in high-energy stable root. This makes non-linear system more favorable over linear system. In addition to this advantage, nonlinear systems are more efficient in power production than the linear systems. This will be further discussed in section 3.

1.3 Overview of the Thesis

A flexible and accurate test bench to measure power and voltage is needed because many designs for MEMS energy harvester are being researched and it is crucial that the test bench is able to test the device and also collect accurate power and voltage data. Graphs such as power vs. resistance and voltage vs. frequency are very important to analyze the performance of the MEMS device, and accurate plots are needed to develop an efficient and practical MEMS device. Having a flexible and accurate test bench will allow different designs of MEMS device to be tested and analyzed accurately and help researchers characterize the system built and create the most optimal MEMS energy harvester.

The main role of this thesis is to serve as a step by step manual that helps users characterize and analyze energy harvesters. The thesis will start out by explaining the test bench design, and after the overall setup is explained, some of the key devices will be discussed. Afterwards, experiment steps to characterize energy harvesters will be explained and properties of linear and nonlinear systems will be further discussed. In the end, experiment results of MIDE V21BL cantilever piezoelectric energy harvester will be analyzed and used to describe the accuracy of our test bench.

2 Design of the Test System:

2.1 Overall Layout of the Test System

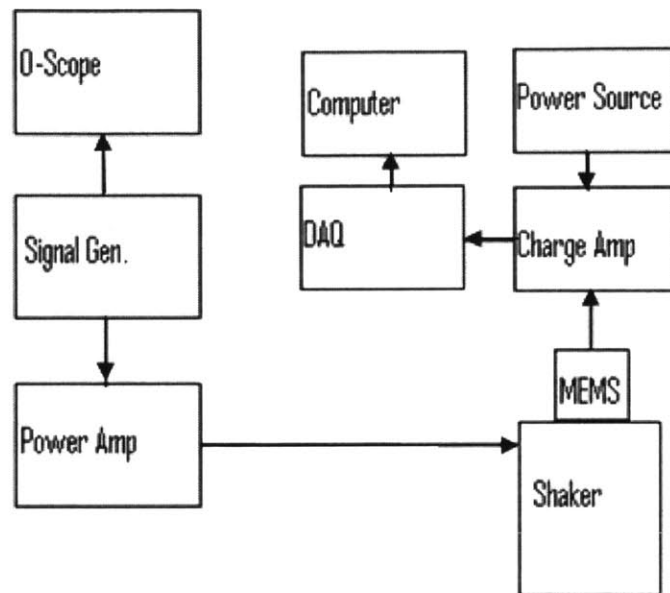


Figure 2-1: A diagram of the overall layout of the test bench. The arrows represent the direction of the signals. Note that MEMS is the energy harvester and is mounted on the shaker.

ET-126-4 electrodynamic shaker was used to simulate vibration and signal was sent to the shaker by a signal generator amplified by a power amplifier. Also, the signal created by the signal generator was connected to an oscilloscope so the signal being sent could be visualized and seen on a screen.

The energy harvester was mounted on top of the shaker and connected to a charge amplifier, and the charge amplifier was connected to a DAQ board. The DAQ board was connected to a computer using USB and was used to read the values from the charge amplifier. Also, power source was used to power the charge amplifier.

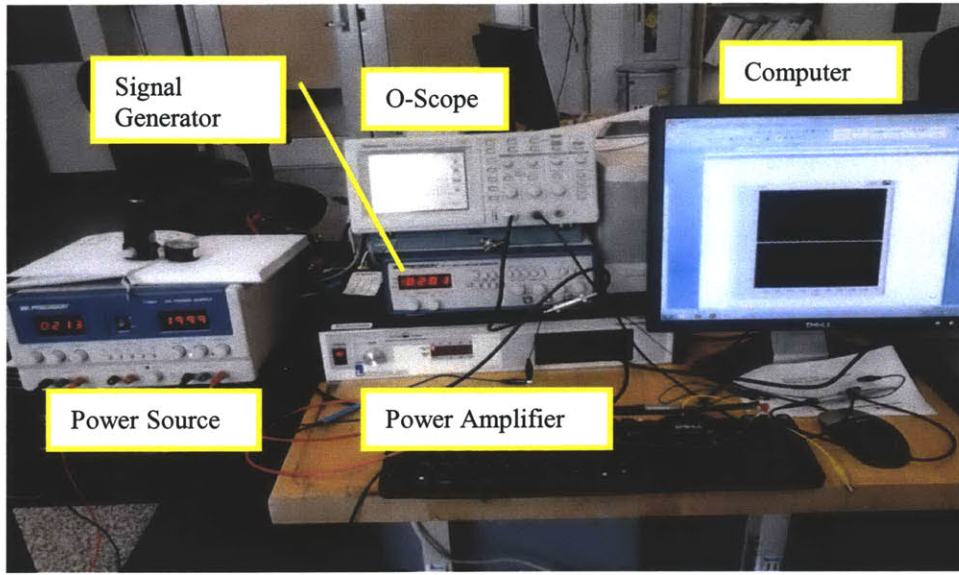


Figure 2-2: Test bench layout with labeled machinery.

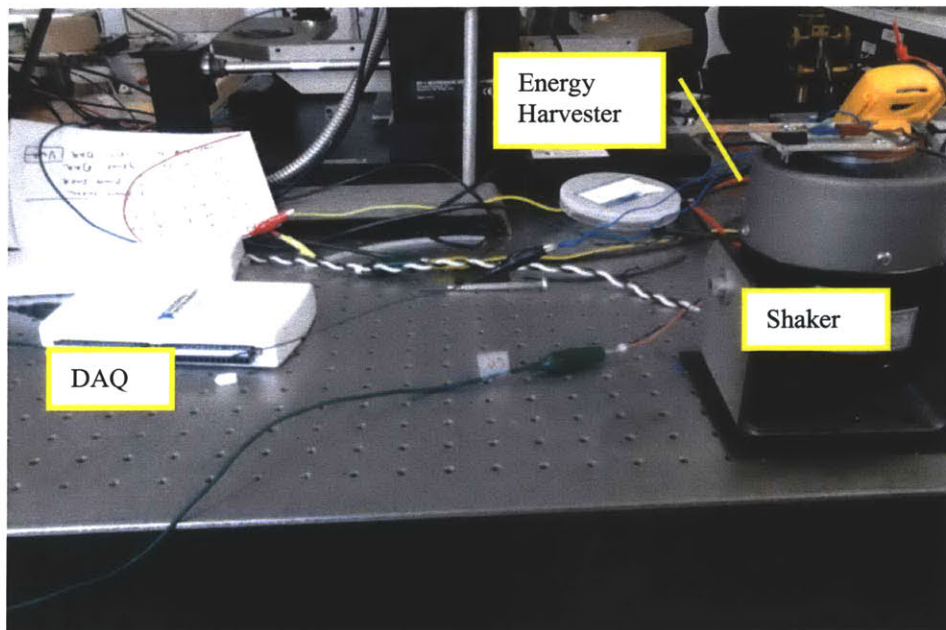


Figure 2-3: Test bench layout with labeled machinery.

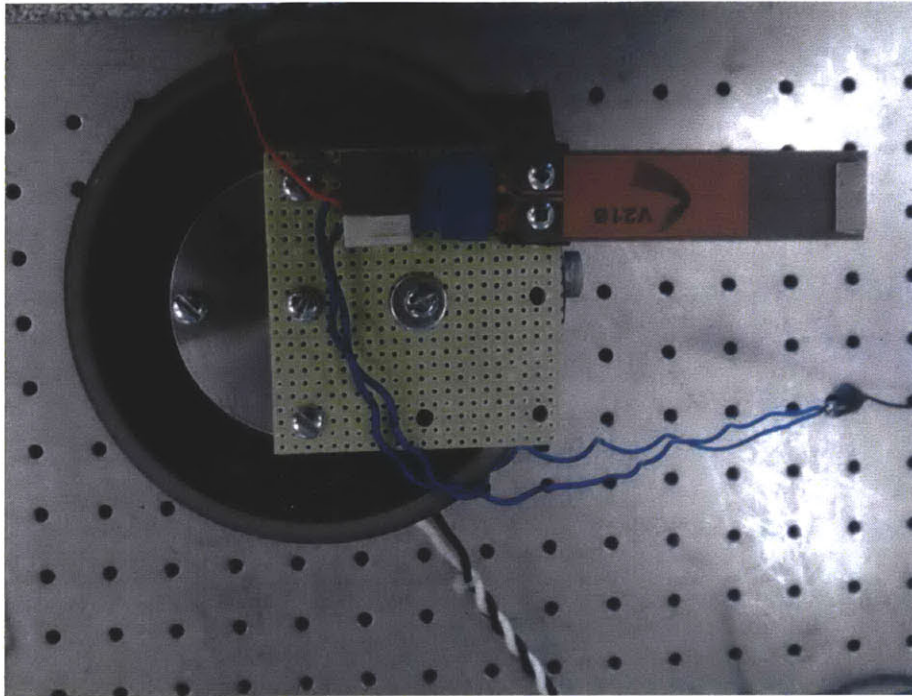


Figure 2-4: Energy harvester mounted on the shaker.

2.2 Details Regarding Shaker

ET-126-4 electrodynamic shaker is a small permanent magnet shaker that has a 2.125 inch diameter table with multiple attachment points. The shaker has a 0.75 inch stroke, frequency range of up to 8,500 Hz, and peak force of 13 lb-f, which is about 57.83 N. Further specifications of ET-126-4 can be seen on Appendix B. This shaker was used because it uses a permanent magnet and this allows the shaker to be more accurate than electric power source magnet and prevents the shaker from overheating.

To setup the shaker, the shaker was bolted down to the test bench and positive and negative nodes of the power amplifier were connected to the shaker's input source.

2.3 Details Regarding Charge Amplifier

The charge amplifier used in this setup was a 5000B-100A charge amplifier with a gain of 100mV/pC. To setup the amplifier, a coaxial cable with positive and negative nodes was connected to the 10-32 input connector coaxial on the charge amplifier, and these positive and negative input nodes were connected to the positive and negative nodes of the energy harvester.

The power and output side of the amplifier was assembled by connecting Vout to the Analog Input1 of DAQ board's input, Ground to the negative node of the power source and ground of the DAQ board's input, +Vcc to the positive node of the power source, and NC to nothing. The wires of Vout, Ground, +Vcc, and NC ports are color coded and they are green, blue, red, and white respectively; a detailed specification sheet for model 5000B is on appendix C.

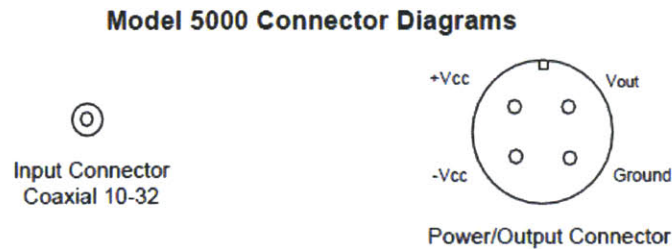


Figure 2-5: Input and output chord of the charge amplifier[9].

The power source for the charge amplifier ranges from 12 to 30 Vdc and the output voltage swing is 70% of the source voltage, which means that the max output from the charge amplifier is 21V. Due to this property, when our energy harvester was tested with the charge amplifier, the output voltage from the charge amplifier was capped because the charge created by the energy harvester was too high and the converted voltage value exceeded the charge amplifier's voltage output limit. Therefore, charge amplifier was not used and open circuit voltage was measured by connecting our energy harvester straight to the DAQ board (this will be discussed further in section 3).

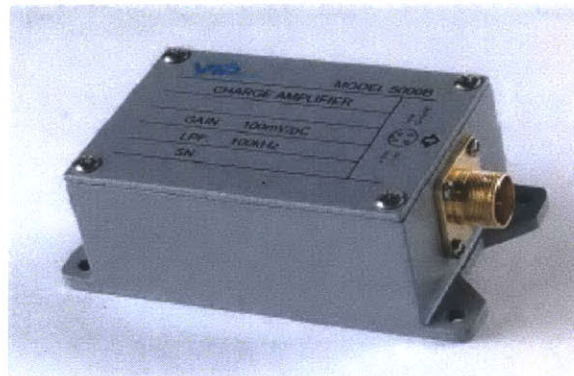


Figure 2-6: 500B-100A charge amplifier with a gain of gain of 100mV/pC [9].

2.4 Details Regarding DAQ Board

To collect data from the energy harvester and analyze it using LabView on a computer, a DAQ board was used to collect data from the energy harvester. The DAQ board receives analog input signals from the energy harvester, and then transfers these signals into data that can be displayed and analyzed on LabView. The DAQ board used for this experiment was NI USB-6210, a 16-Bit, 250 Kilo samples per second Multifunction DAQ board. This DAQ board also has two analog input modes one being -10V to 10V and the other being -200mV to 200mV. The voltage range accuracy and range sensitivity is 2.69mV and 91.6 μ V, and .088mV and 4.8 μ V respectively. A detailed specification sheet for NI USB-6120 is on appendix D. This DAQ board was chosen since it will be sensitive enough for our piezoelectric energy harvester and will take enough number of samples to get an accurate measurement.

3. Experimental Evaluation

3.1 Specification of Energy Harvester Device

The energy harvester device used for this experiment setup is a V21BL piezoelectric vibration energy harvester by MIDE technology. The device is a linear system and is a simple cantilever beam with 1 gram tungsten proof mass attached on its tip using epoxy.

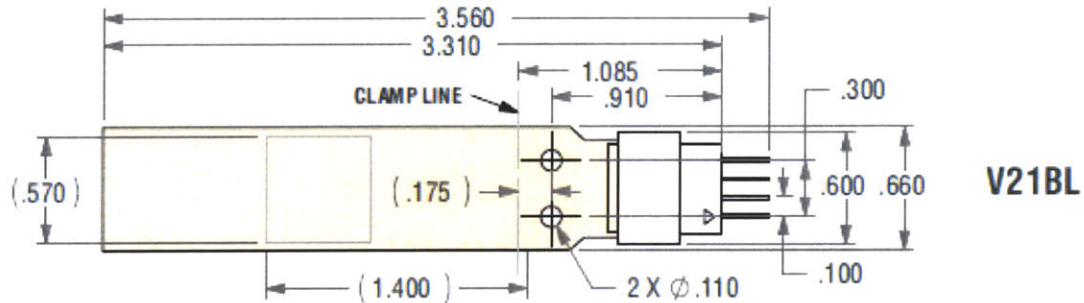


Figure 3-1: Diagram of V21BL energy harvester; measurements are in inches [10].

V21BL is a bimorph with a thickness of .031in and has two layers of piezoelectric material that are each connected to two prongs, one positive and one negative. Counting from the bottom, the first and third prongs in the diagram above are positive nodes and the second and fourth prongs are negative nodes. The max deflection of V21BL is .18in, and further specifications are in appendix E.

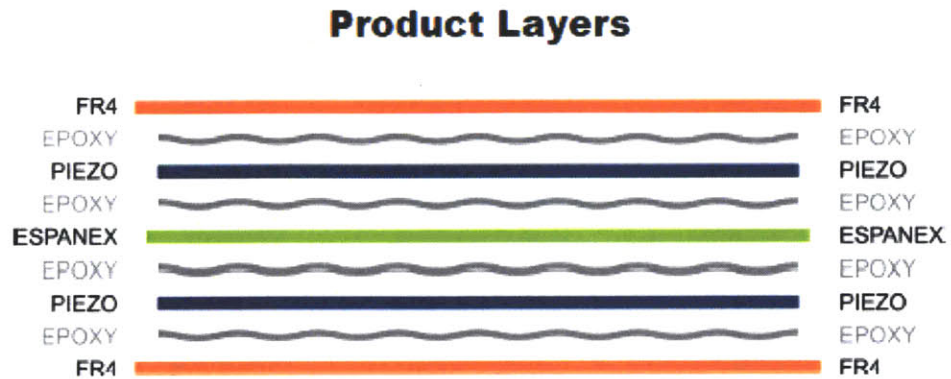


Figure 3-2: Layers of V21BL. The two piezoelectric materials on both sides of the cantilever beam make V21BL bimorph [10].

As the weight of proof mass increases, the resonant frequency for this system decreases, and this pattern can be seen in the plot published by the manufacturer. From this plot it can also be seen that the resonant frequency for our system with 1 gram of proof mass is around 76Hz.

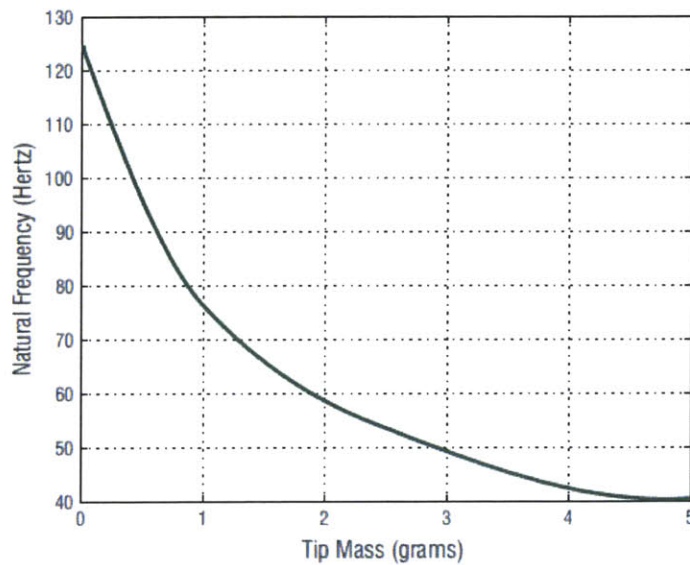


Figure 3-3: Graph that shows the relationship between natural frequency and proof mass. As mass increases, natural frequency decreases [10].

3.2 Open Circuit Measurements for the Energy Harvester

As mentioned in section 2.3, although we planned on measuring the charge created by the energy harvester by using the charge amplifier, the charge amplifier was not used because the charge created by the energy harvester was too high and the converted voltage value exceeded the charge amplifier's voltage output limit. Instead, open circuit voltage of the energy harvester was measured by connecting the energy harvester directly to the DAQ board. To measure the open circuit voltage, the positive and negative nodes of the energy harvester were clamped and connected directly into Input 1 and Ground of the DAQ board.

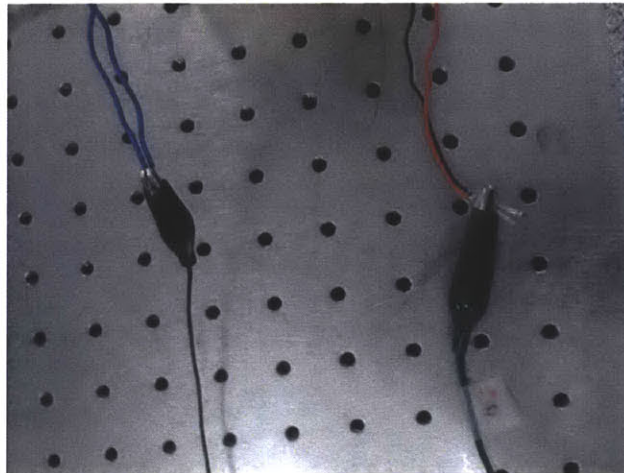


Figure 3-4: Positive and negative nodes of the energy harvester connected to clamps that are connected to Input 1 and Ground of the DAQ board.

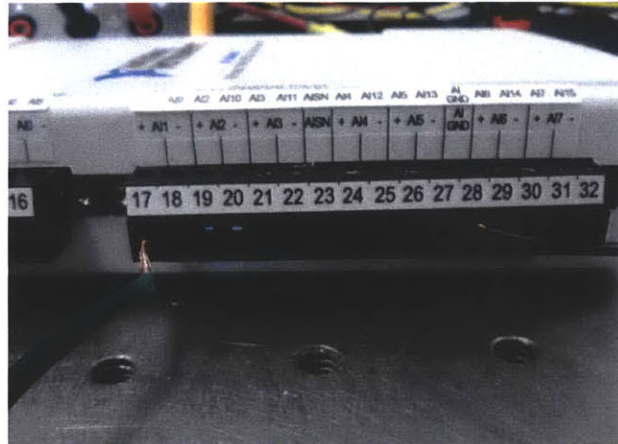


Figure 3-5: Green wire inserted in Input1 and black wire inserted in Ground of the DAQ board.

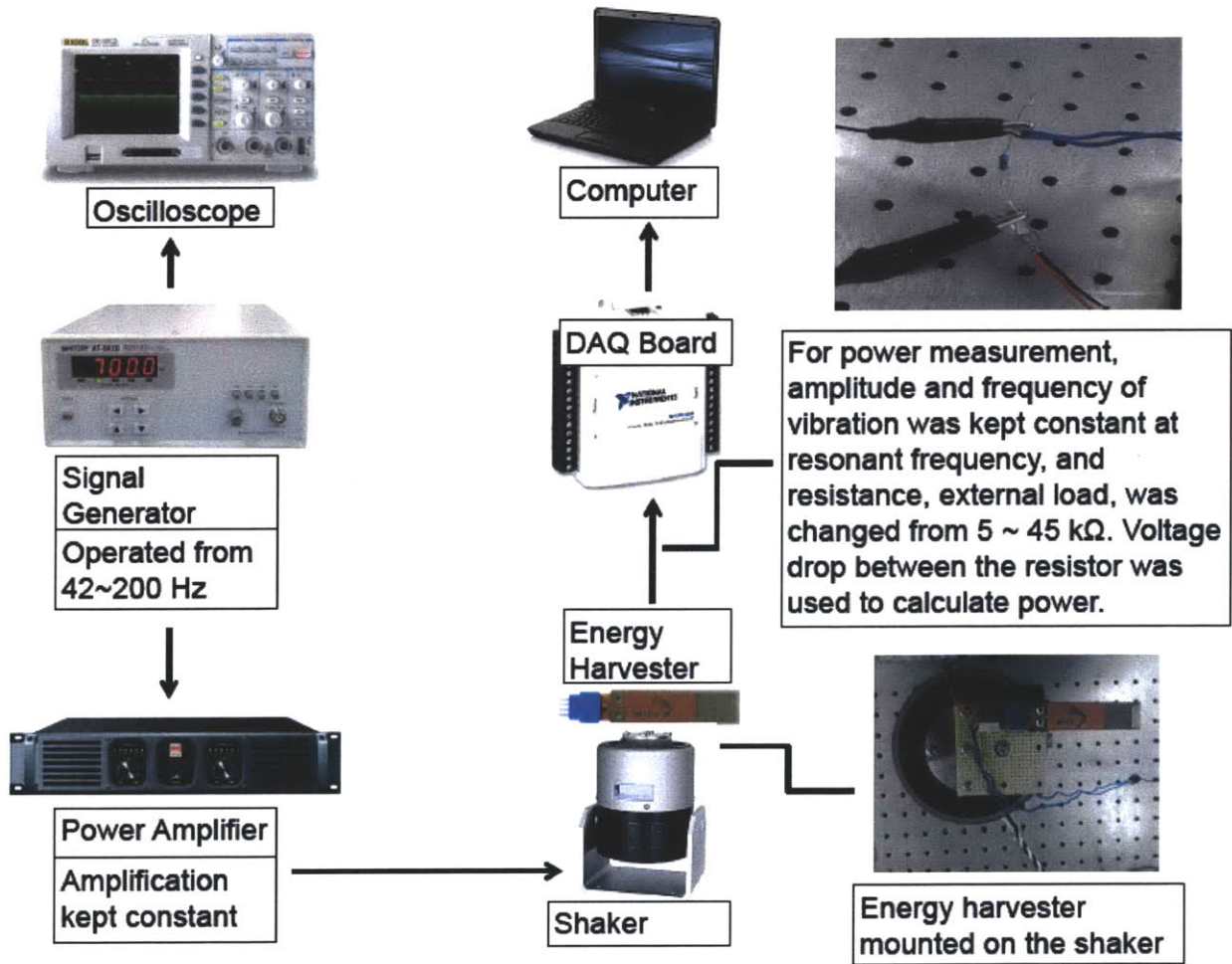


Figure 3-6: A diagram of overall layout of test bench without charge amplifier. Explanations for how the voltage and power were measured are written in the diagram.

In order to record the voltage measurements using LabView, a simple waveform graph and block diagram that graphs and measures the voltage input were created; steps on how the waveform graph and block diagram were made and LabView is set up are shown in Appendix A.

Since two variables that affect piezoelectric energy harvester are frequency and amplitude of vibration, the open circuit voltage was measured by sweeping the frequency from 42Hz to 200Hz while the amplitude was kept constant by keeping the power amplifier at a constant level. To be more specific, the power amplifier was set to a level such that the max voltage amplitude at 67Hz was 8.6V. One of the open circuit voltage measured on LabView is shown below.

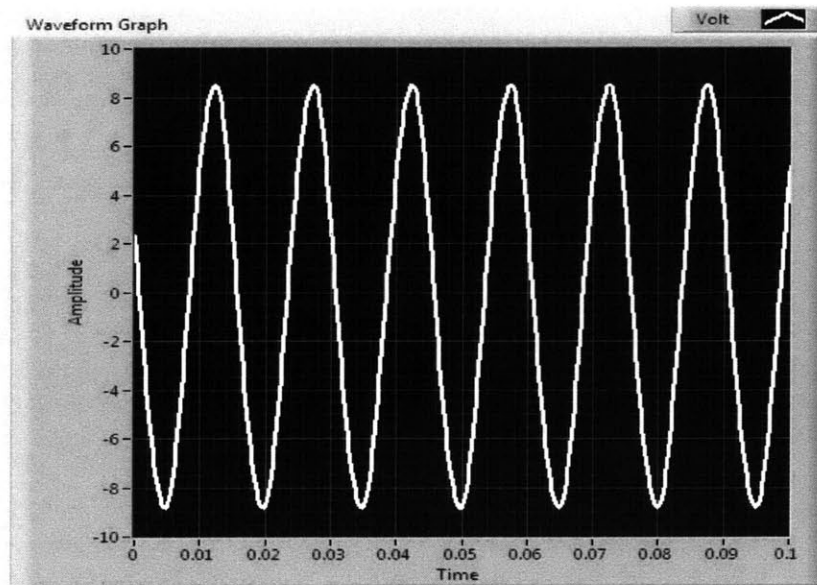


Figure 3-7: Open circuit voltage measured at 67Hz.

The frequency sweep was made for 21 different frequency points, and the data gathered are shown in the in Table 3-1.

TABLE 3-1: Open circuit voltage created by the energy harvester for given frequency.

Hz	Volts	Hz	Volts	Hz	Volts
42	0.6	69	7.75	90	0.95
55	1.25	71	5.65	95	0.8
62	2.1	72	4.85	100	0.7
65	3.6	75	3.3	115	0.45
66	4.35	77	2.2	120	0.35
67	8.6	80	1.8	160	0.25
68	8.35	86	1.2	200	0.1

From looking at the table it can be seen that the energy harvester's resonance frequency is at 67Hz. To further analyze the data, a plot can be made to visualize the relationship between frequency and open circuit voltage.

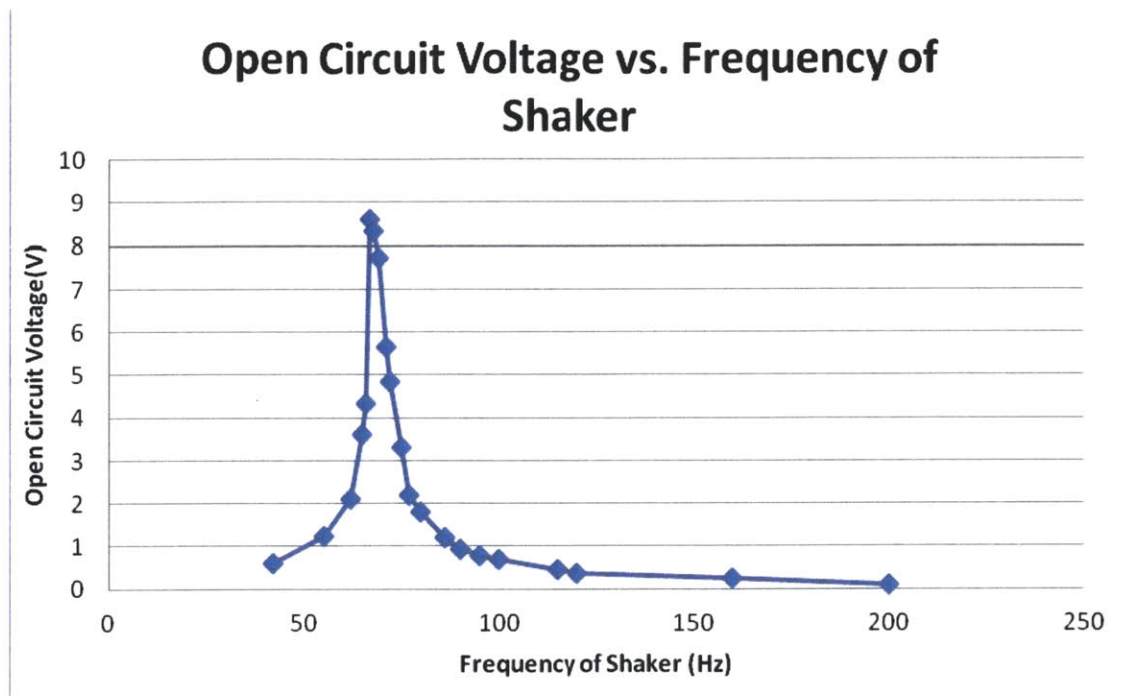


Figure 3-8: Plot of open circuit voltage vs. frequency for a V21BL with resonance frequency of 67Hz and bandwidth of 8Hz. The graph shows narrow bandwidth and sensitivity of open circuit voltage to the change in frequency. The shape of the graph is similar to that of Figure 1-4.

From looking at the graph above, bandwidth can be found by finding the difference between two frequency values at half of max open circuit voltage value. In the plot above, it can be analyzed that V21BL has a small bandwidth range of about 8Hz, quality factor, which is resonance frequency divided by the bandwidth, of about 8.375, and the outputs near resonant frequency are very sensitive to the change in frequency. The graph above is similar to Figure 1-5 discussed in section 1.2.1. This was expected since V21BL is a linear system, and small bandwidth and strong sensitivity to frequency are traits that belong to linear systems. This result shows that our test bench is accurate and was able to correctly characterize a linear system.

3.3 Theoretical Calculation of Power

Maximum power that can be created by the energy harvester is one of the most important values of the harvester. After doing the frequency sweep to gather voltage vs. frequency data, resonant frequency can be found, and using this resonant frequency, max power can be found experimentally or using theoretical calculation.

In theory, maximum power is achieved when the external impedance is equal to internal impedance. This can be shown by analyzing a simple circuit diagram as shown below.

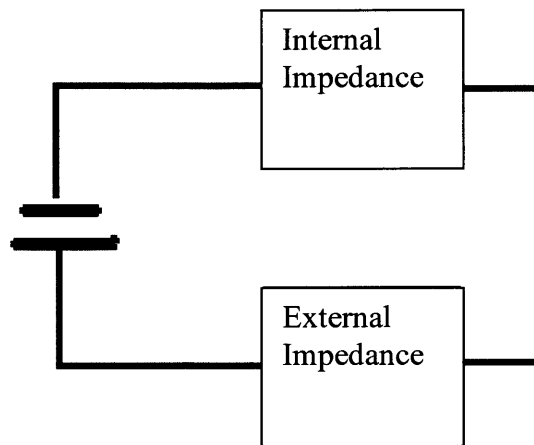


Figure 3-9: Series circuit with voltage source and internal and external impedance.

The voltage source, internal impedance, and external impedance in the circuit diagram above represent: voltage created by the energy harvester without considering the internal resistance of the energy harvester, internal resistance that exists in the energy harvester itself, and resistance from external load exerted on the energy harvester respectively. Given that power can be expressed by the following equation:

$$P = IR^2 = \frac{V^2}{R} \quad (3-1)$$

Power exerted on the external load can be expressed by the following:

$$P_{\text{ext}} = \frac{\left[\left(\frac{Z_{\text{ext}}}{Z_{\text{ext}}+Z_{\text{int}}}\right)V\right]^2}{Z_{\text{ext}}} = \frac{Z_{\text{ext}}}{(Z_{\text{ext}}+Z_{\text{int}})^2} V^2 \quad (3-2)$$

If constant values C1 and C2 are assigned to Z_{int} and V respectively, the following pattern can be seen for a P_{ext} vs. Z_{ext} plot:

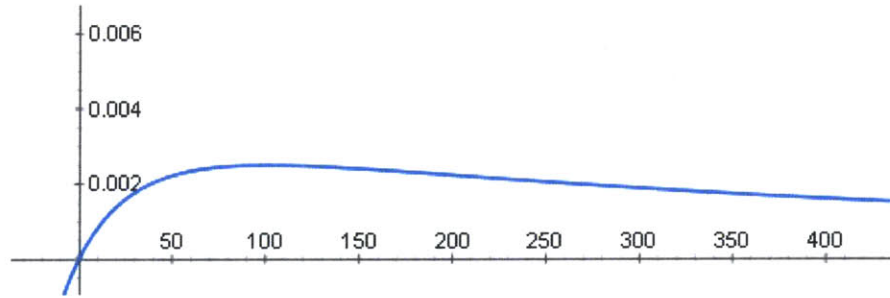


Figure 3-10: Pattern seen from plotting $P_{\text{ext}}(Z_{\text{ext}})$ function such as equation 3-2.

When equation for P_{ext} is differentiated by Z_{ext} , it can be seen that P_{ext} is at maximum when Z_{ext} is equal to Z_{int} .

$$\frac{\partial P_{\text{ext}}}{\partial Z_{\text{ext}}} = \frac{Z_{\text{int}}^2 - Z_{\text{ext}}^2}{(Z_{\text{int}} + Z_{\text{ext}})^4} \quad (3-3)$$

This shows that for a linear system, the max power created by the energy harvester is limited by the internal impedance of the energy harvester. Unlike the linear system, nonlinear

system's max power is not limited by the internal impedance and this is another advantage that a nonlinear system has over the linear system.

3.4 Experimental Measurement of Power

Maximum power output by this energy harvester can also be calculated experimentally by doing a resistance sweep. With the shaker set at resonance frequency of 67 Hz and power amplifier set at a constant level, resistors can be connected between the positive and negative nodes of the energy harvester as shown below and the voltage on different external loads can be measured.

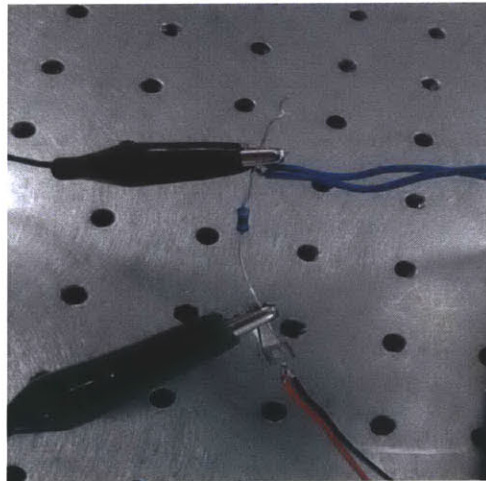


Figure 3-11: Resistor connecting the positive and negative nodes of energy harvester, and DAQ board measuring the voltage drop between the resistors by connecting to the ends of the resistor.

For our resistance swap the frequency was set at the resonant frequency, 67Hz, and power amplifier was set at a level such that open circuit voltage at 67Hz was 10.3 V. In addition, a resistor connected in series to a potentiometer was used as the external load so resistance could be set easily for different values.

For different external loads, the voltage drop was measured and using equation 3-1, power created at each load was measured. Data gathered from the resistance swap is shown in Table 3-2.

TABLE 3-2: Power values calculated from the resistance swap

Voltage(V)	Resistance(Ω)	Power(Watt)
2.2	5000	9.68E-04
4.1	10000	1.68E-03
5.6	15020	2.09E-03
6.3	17000	2.33E-03
6.55	18000	2.38E-03
6.7	19000	2.36E-03
7.3	22000	2.42E-03
7.8	25000	2.43E-03
8.2	28000	2.40E-03
9	35000	2.31E-03
9.65	45000	2.07E-03

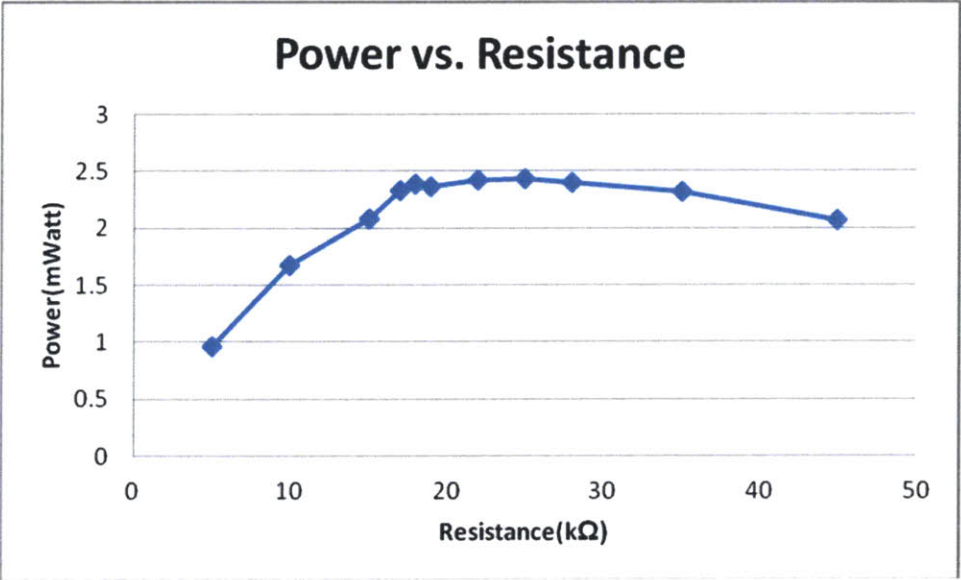


Figure 3-12: Graph that plots power vs. resistance data from table 3-2.

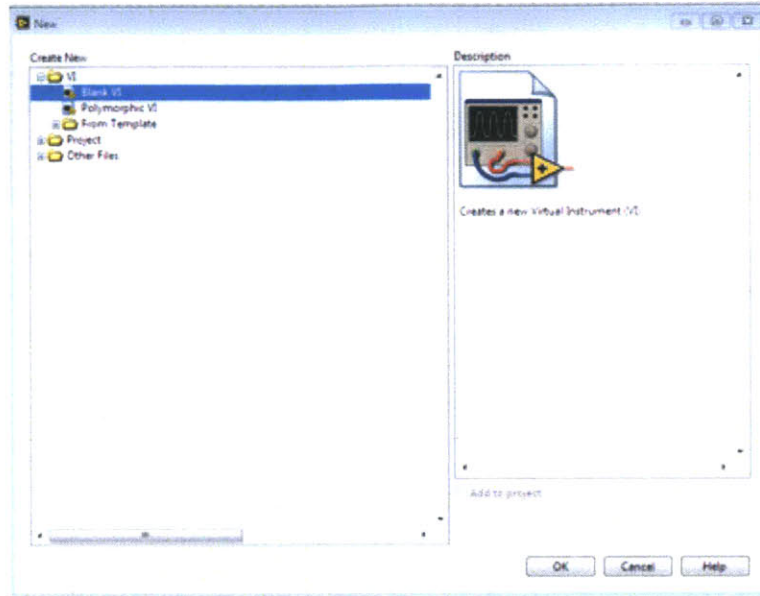
From the resistance sweep plot, it can be seen that the maximum power of 2.43mWatts is at the external load of around 25 k Ω . As shown in equation 3-3, max power is obtained when internal load is equal to external load. Using this fact, the internal impedance of the energy harvester at 67Hz is about 25k Ω .

4. Summary and Conclusion

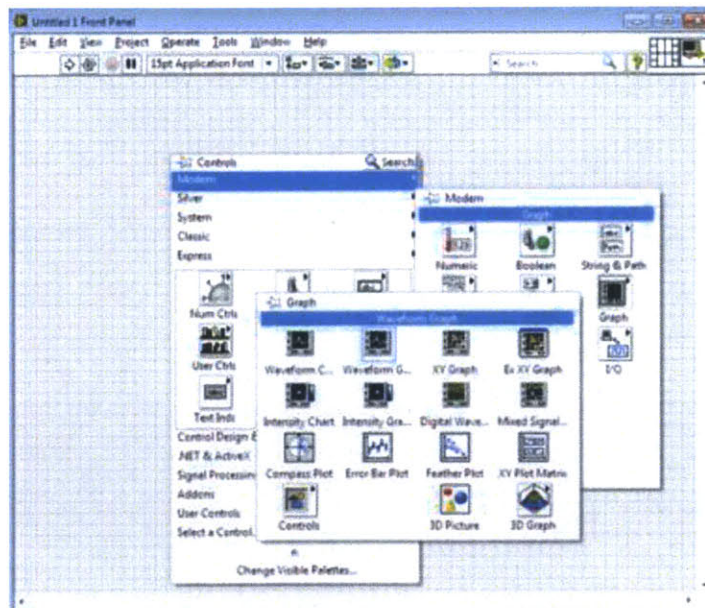
To facilitate the development of piezoelectric MEMS energy harvesters, a test bench was developed to test and analyze the different designs of piezoelectric MEMS energy harvester. The test bench created is able to accurately collect data and measure open circuit voltage, resonance frequency, max power output, and current, and will be helpful in testing many different types of energy harvester designs. For the V21BL energy harvester tested, open circuit voltages, max power output, and resonance frequency could be measured. However, charge was not measured because the charge created by the energy harvester was too high for the charged amplifier to convert it to its output voltage range. The charge amplifier, however, will work for a MEMS energy harvester since the charge created by a MEMS energy harvester is many magnitudes smaller than the charge created by V21BL.

In our test bench, the power amplifier was kept at a constant value so the amplitude of a frequency could be kept constant. However, the amplitude of a frequency is another important factor that affects piezoelectric energy harvesters' output values, and accelerometer should be used to analyze how force exerted affects the values of open circuit voltage, max power output, and charge. Although we did not include an accelerometer in our test bench, accelerometer can be easily attached to the shaker and connected to the DAQ board to further improve the test bench.

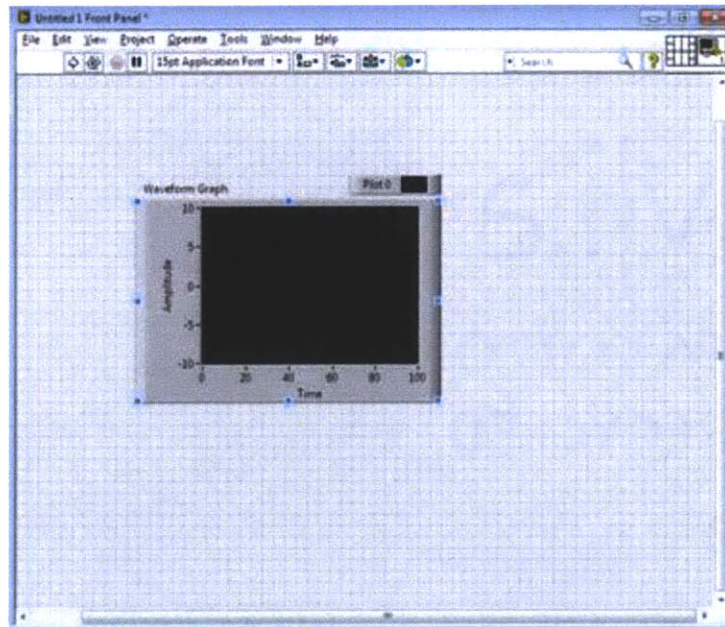
Appendix A – LabView Setup



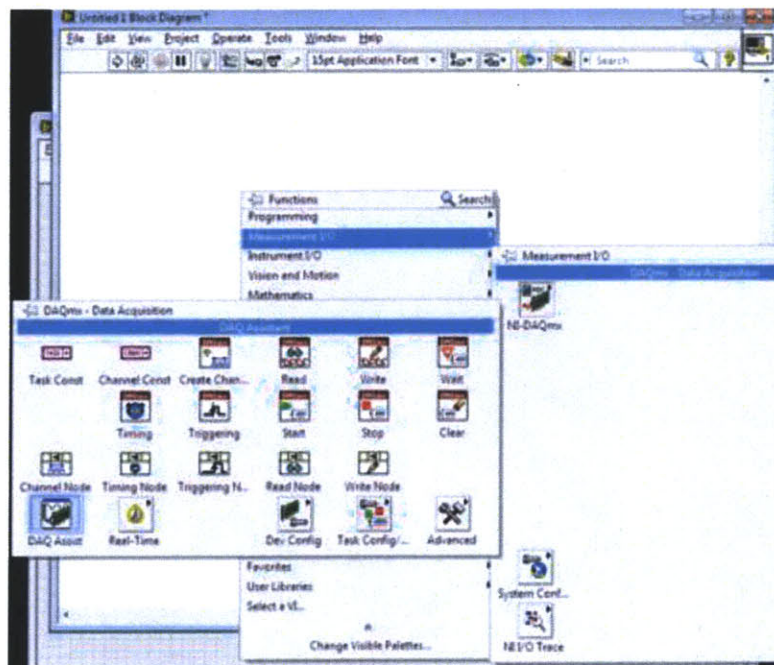
Step 1: Open LabView and create a blank form.



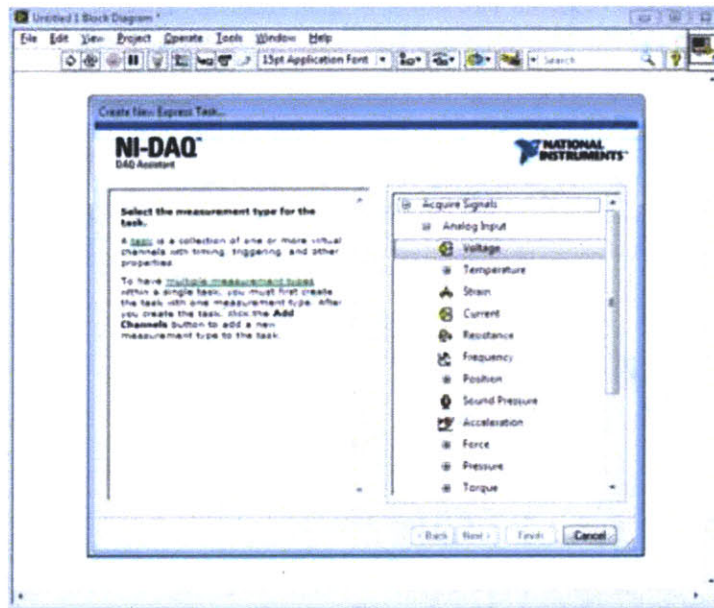
Step 2: Right click on the screen and press modern, graphs, and waveform graph.



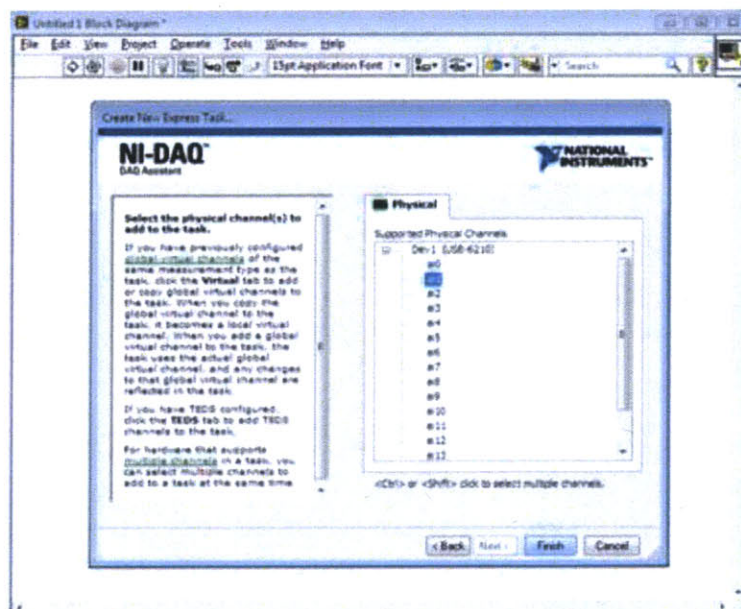
Step 3: Following Graph will be shown on the panel.



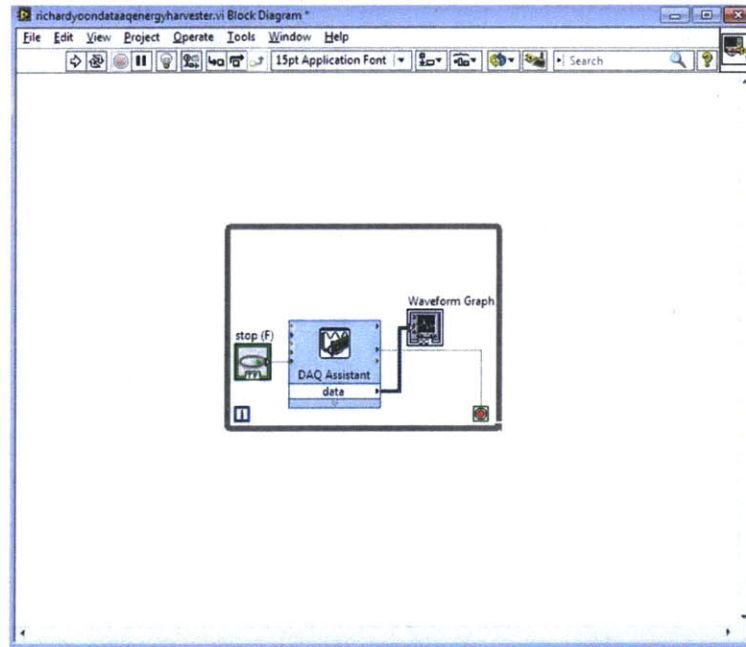
Step 4: Open up a block diagram platform and right click and click on Measurement I/O, DAQ max, and then click on DAQ Assist.



Step 5: After clicking on the DAQ Assist block diagram, following box will show. Click on the type of input the DAQ board will be receiving, which is voltage for our experiment.

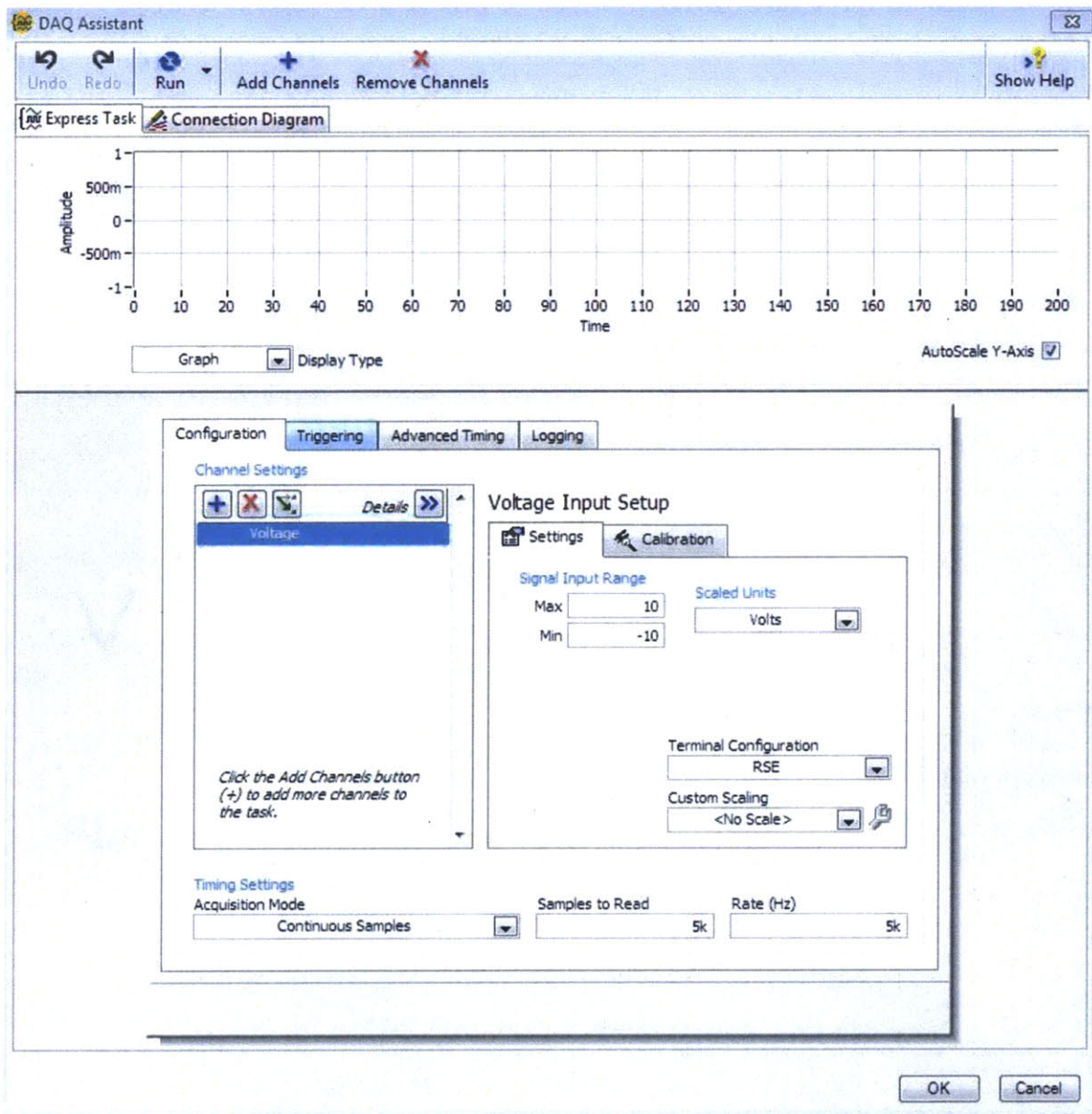


Step 6: Choose which ports it will be taking the input from and press finish, ai1 for our experiment.

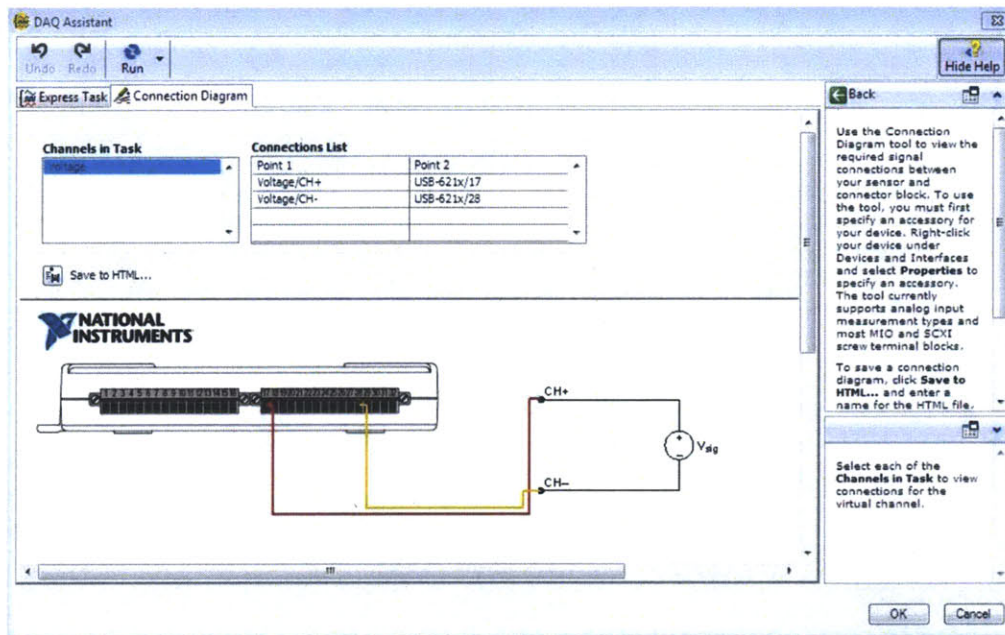


Step 7, Connect the waveform graph to the data source of DAQ Assistant. Block diagram is now finished.

Before measuring the voltage, measurement settings have to be set for the DAQ Assistant. Double click on the DAQ Assistant in the block diagram and set the following values: Max and Min of Signal Input Range to 10 and -10 respectively, Scaled Units to Volts, Terminal Configuration to RSE, Acquisition Mode to Continuous Samples, Samples to Read to 5K, and Rate to 5K.



Step 8: Setting the correct measurement setting for the DAQ measurement system.



Step 9: The DAQ assistant has a Connection Diagram tab that shows how the wires should be connected to the DAQ board. Look at this diagram to double check the wires are connected correctly.

Appendix B – ET-126 Shaker Specifications



>> [Home](#)

ET-126-1,-4
ET-126HF-1,-4



- 25 pounds pk sine force
- .75 inch stroke
- 2.125 inch diameter table
- Low stray magnetic field
- Frequency range DC - 8.5 KHz
DC - 14 KHz
- (HF)
- Trunnion mounting base

The Labworks ET-126 Electrodynamic Transducer is a rugged, full featured, small permanent magnet shaker. It is ideally suited for the production screening of small components, engineering design verification/evaluation, or for larger transducer calibration systems. The shaker features a 2.125 inch diameter table with multiple attachment points, and an extraordinary 0.75 inch stroke. The ET-126 has a linearly compliant armature suspension that is also suitable for modal testing with a current source amplifier. The ET-126HF (High Frequency) with its slightly heavier armature has an extended full force frequency range of up to 14 KHz with operation to 20 KHz at 7 lbf pk sine, and a dual thread center mounting hole with #10-32 threads for mounting accelerometers and other vibration transducers. Available in two different impedance ranges, the ET-126 series are easily matched to most amplifiers yielding the maximum system performance.

General Specifications



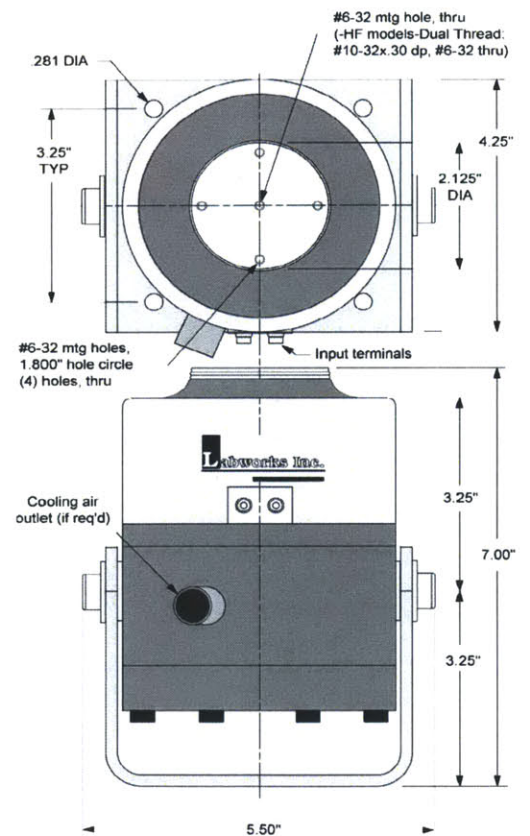
Performance	ET-126-1,-4	ET-126HF-1,-4
Sine force		
Natural cooling	13 lbf pk	13 lbf pk
With cooling vacuum*	25 lbf pk	25 lbf pk
Random force		
Natural cooling	8 lbf rms	8 lbf rms
With cooling vacuum*	17.5 lbf rms	17.5 lbf rms
Shock force	53 lbf pk	53 lbf pk
Frequency Range	DC-8,500Hz	DC-14 KHz(-20 KHz, 7lbf)
Max displacement		
Continuous pk-pk	.75 in	.50 in
Between stops	.75 in	.50 in
Maximum velocity	120 ips pk	100 ips pk
Physical		
Armature weight	0.20 lbs	0.35 lbs
Suspension stiffness	15 lb/in	15 lb/in
Dimensions	6.5"H x 4.8"W x 4.25"D	6.5"H x 4.8"W x 4.25"D
Shaker weight	11 lbs	11 lbs
Impedance		
	ET-126-1, ET-126HF-1	ET-126-4, ET-126HF-4
Nominal E/I	1.3 Ohm	2.9 Ohm

Options

[SI-126 Vibration Isolation Mounts](#)

[MS-129 Modal Stinger Kit](#)

[*CB-152 Cooling vacuum, required for operations above 13 lbf](#)



Appendix C – Charge Amplifier Specifications



Quality

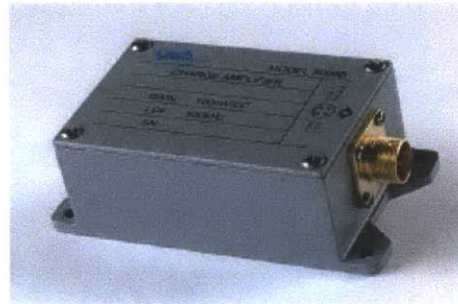
Innovations

Customer Satisfaction

Charge Amplifier Module

MODEL 5000

- Small Size, Rugged Construction
- High Gain
- Wide Bandwidth
- Fixed Low Pass Filter
- Adjustable Sensor Sensitivity
- Output Short Circuit Protection

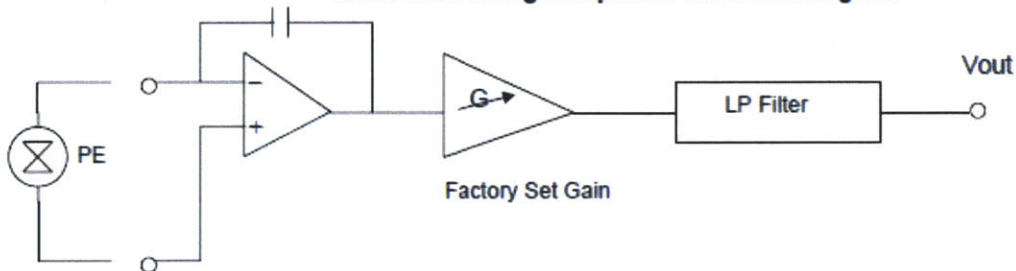


Description

The VIP Sensors Charge Amplifier Model 5000 accepts signals from piezoelectric type of transducers and converts the high impedance charge input into a low impedance voltage output signal. The signal is processed through a gain stage and a 2-pole low pass filter stage. The value for gain and the corner frequency for the low pass filter are set at the factory.

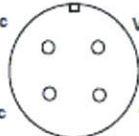
The Model 5000A requires a \pm voltage source from 6 to 15 Vdc and its output voltage swing is about 70% of the source voltage. The Model 5000B operates from a single positive voltage source from 12 to 30 Vdc; an internal voltage divider halves the source voltage to bias its circuitry and its output voltage signal.

Model 5000 Charge Amplifier Functional Diagram



Model 5000 Connector Diagrams


Input Connector
Coaxial 10-32


Power/Output Connector

Page 1 of 2

VIP Sensors
California, USA

Ph (949) 429 3558
Fx (949) 528 0126

info@vipsensors.com
www.vipsensors.com

VIP Sensors reserves the right to modify
these specifications without notice. V01

Charge Amplifier Module

MODEL 5000

SPECIFICATIONS

The following performance specifications are at +75°F (+24°C), unless otherwise noted.

	UNITS	
INPUT		
Type		Piezoelectric, single-ended
Capacitance	pC	1000 Maximum
Resistance	MΩ	20
OUTPUT		
Type		Single-ended
Voltage (peak)	%	70 of the maximum supply voltage for model 5000A
	%	70 of ½ the maximum supply voltage for model 5000B
Current	mA	10 maximum
TRANSFER CHARACTERISTICS		
Gain	mV/pC	10 to 100 Set at factory; default value 100
Accuracy	%	± 1 maximum for 1 Hz to 100 kHz at 24°C
	%	± 2 maximum for 1 Hz to 100 kHz over Operating Temp Range
Low Pass Filter	Hz	F (-3 ±1dB): 1 to 100,000 set at factory 2 poles, -12dB/octave roll off
Noise	μV rms	≤ 10 RTI
Harmonic Distortion	%	< 1 at 10 kHz with 10 nF capacitive load and full-amplitude output
Broadband Frequency Response		
Low Cutoff Frequency	Hz	F (-3 ±1dB): 1 Attenuation Rate: 6dB/Oct
Upper Cutoff Frequency	Hz	F (-3 ±1dB): ≤ 100,000 Attenuation Rate: 12dB/Oct
ENVIRONMENTAL		
Temperature	°F (°C)	Operating temperature: +32 to +104 (0 to +40) Storage temperature: -67 to +185 (-55 to 85)
Humidity	%	95 maximum relative humidity
POWER SUPPLY		
Power Sources	Vdc	± 6 to ± 15 for Model 5000A +12 to +30 for Model 5000B
PHYSICAL CHARACTERISTICS		
Dimensions	inches (mm)	2.0W × 1.3H × 3.9L (50 × 32 × 100)
Weight	oz (grams)	8.8 (250)
Connections		4-pin Power/Output connector 10-32 Transducer Input receptacle
ACCESSORIES		4-pin Power/Output Cable
ORDERING INFORMATION		
Model 5000X - yyy		X = A (± 6 to ± 15 Vdc supply) or B (+12 to +30 Vdc supply) yyy = Gain (010 to 100)

Appendix D – NI USB-6210 DAQ Board Specifications

NI USB-6210

16-Bit, 250 kS/s M Series Multifunction DAQ, Bus-Powered

- 16 analog inputs (16-bit, 250 kS/s)
- 4 digital inputs; 4 digital outputs; two 32-bit counters
- Bus-powered USB for high mobility; built-in signal connectivity
- NI signal streaming for sustained high-speed data streams over USB
- Compatibility with LabVIEW, LabWindows™/CVI, and Measurement Studio for Visual Studio .NET
- NI-DAQmx driver software and LabVIEW SignalExpress LE interactive data-logging software



Overview

The NI USB-6210 is a bus-powered M Series multifunction data acquisition (DAQ) module for USB that is optimized for superior accuracy at fast sampling rates. It offers 16 analog inputs; a 250 kS/s single-channel sampling rate; four digital input lines; four digital output lines; four programmable input ranges (± 0.2 to ± 10 V) per channel; digital triggering; and two counter/timers.

The USB-6210 is designed specifically for mobile or space-constrained applications. Plug-and-play installation minimizes configuration and setup time, while direct screw-terminal connectivity keeps costs down and simplifies signal connections. This product does not require external power.

This module also features the new NI signal streaming technology, which gives you DMA-like bidirectional high-speed streaming of data across USB. For more information about NI signal streaming, view the Resources tab.

Bus-powered M Series devices for USB are available in OEM versions. Check the Resources tab or use the left navigation to get pricing and technical information.

Driver Software

NI-DAQmx driver and measurement services software provides easy-to-use configuration and programming interfaces with features such as the DAQ Assistant to help reduce development time. Browse the information in the Resources tab to learn more about driver software or download a driver. M Series devices are not compatible with the Traditional NI-DAQ (Legacy) driver.

Application Software

Every M Series DAQ device includes a copy of NI LabVIEW SignalExpress LE data-logging software, so you can quickly acquire, analyze, and present data without programming. In addition to LabVIEW SignalExpress, M Series DAQ devices are compatible with the following versions (or later) of NI application software: LabVIEW 7.1, LabWindows/CVI 7.x, or Measurement Studio 7.x. M Series DAQ devices are also compatible with Visual Studio .NET, C/C++, and Visual Basic 6.0.

The mark LabWindows is used under a license from Microsoft Corporation. Windows is a registered trademark of Microsoft Corporation in the United States and other countries.

Specifications

Specifications Documents

- Specifications (2)
- Data Sheet

Specifications Summary

General

Product Name	USB-6210
Product Family	Multifunction Data Acquisition
Form Factor	USB
Part Number	779675-01
Operating System/Target	Linux , Mac OS , Windows
DAQ Product Family	M Series
Measurement Type	Voltage
RoHS Compliant	Yes
Analog Input	
Channels	16 , 8
Single-Ended Channels	16
Differential Channels	8
Resolution	16 bits
Sample Rate	250 kS/s
Max Voltage	10 V
Maximum Voltage Range	-10 V , 10 V
Maximum Voltage Range Accuracy	2.69 mV
Maximum Voltage Range Sensitivity	91.6 μ V
Minimum Voltage Range	-200 mV , 200 mV
Minimum Voltage Range Accuracy	0.088 mV
Minimum Voltage Range Sensitivity	4.8 μ V
Number of Ranges	4
Simultaneous Sampling	No
On-Board Memory	4095 samples

Analog Output

Channels	0
----------	---

Digital I/O

Bidirectional Channels	0
------------------------	---

Input-Only Channels	4
---------------------	---

Output-Only Channels	4
----------------------	---

Number of Channels	4 , 0
--------------------	-------

Timing	Software
--------	----------

Logic Levels	TTL
--------------	-----

Input Current Flow	Sinking
--------------------	---------

Output Current Flow	Sourcing
---------------------	----------

Programmable Input Filters	No
----------------------------	----

Supports Programmable Power-Up States?	Yes
--	-----

Current Drive Single	16 mA
----------------------	-------

Current Drive All	50 mA
-------------------	-------

Watchdog Timer	No
----------------	----

Supports Handshaking I/O?	No
---------------------------	----

Supports Pattern I/O?	No
-----------------------	----

Maximum Input Range	0 V , 5.25 V
---------------------	--------------

Maximum Output Range	0 V , 3.8 V
----------------------	-------------

Counter/Timers

Counters	2
----------	---

Buffered Operations	Yes
---------------------	-----

Debouncing/Glitch Removal	Yes
---------------------------	-----

GPS Synchronization	No
---------------------	----

Maximum Range	0 V , 5.25 V
---------------	--------------

Max Source Frequency	80 MHz
----------------------	--------

Pulse Generation	Yes
------------------	-----

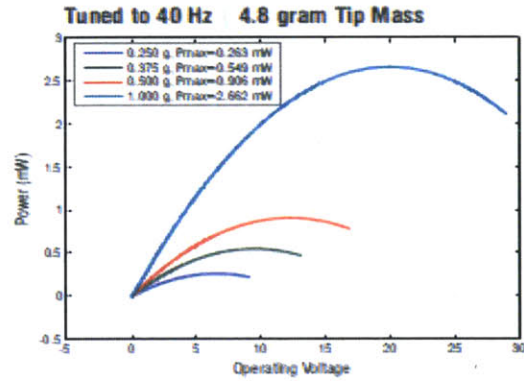
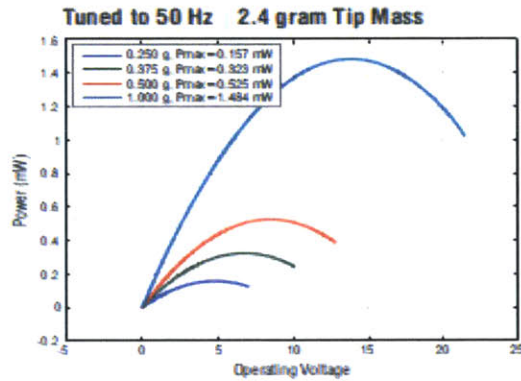
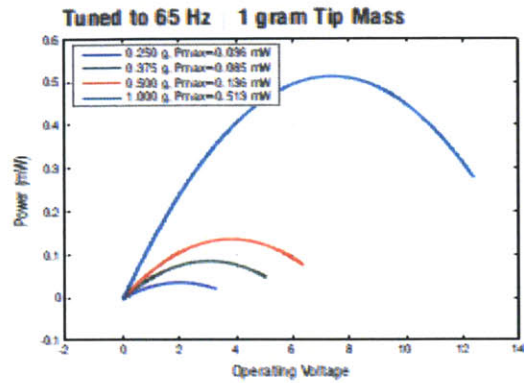
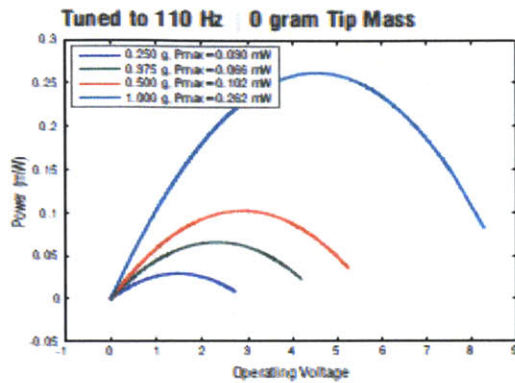
Resolution	32 bits
------------	---------

Timebase Stability	50 ppm
Logic Levels	TTL
Physical Specifications	
Length	16.9 cm
Width	9.4 cm
Height	3.1 cm
I/O Connector	Screw terminals
Timing/Triggering/Synchronization	
Triggering	Digital

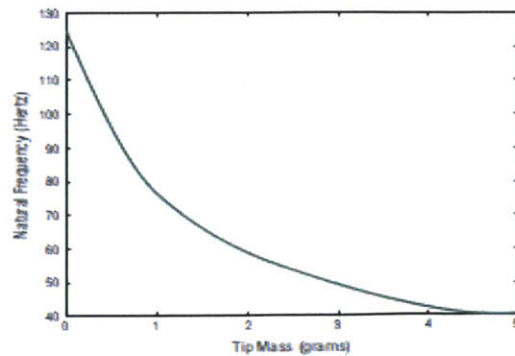
Appendix E –V21BL Specifications



V21BL TYPICAL PERFORMANCE POWER CHARACTERISTICS



V21BL RELATION BETWEEN TIP MASS & NATURAL FREQUENCY



Tip Mass (gram)	F _n (Hz)	Amplitude (g)	Open Circuit Voltage*
0	110	0.25	3.95
0	110	0.375	5.35
0	110	0.5	6.6
0	110	1	12.1
1	65	0.25	8
1	65	0.375	9.9
1	65	0.5	12.4
1	65	1	22.1
2.4	50	0.25	9.8
2.4	50	0.375	13.7
2.4	50	0.5	19.1
2.4	50	1	27.5
4.8	40	0.25	13.2
4.8	40	0.375	19.2
4.8	40	0.5	25.9
4.8	40	1	44.4

* piezo wafers connected in series

Bibliography

- [1] Chau K, Suluff R *et al.* 1998 *Microelectronics Journal* **29** 579-586
- [2] Hajati A 2011 *Ultra Wide-Bandwidth Micro Energy Harvester* Doctor of Philosophy thesis Massachusetts Institute of Technology
- [3] Amirtharajah R and Ch A P 1998 *IEEE Journal of Solid-State Circuits* **33** 687-695
- [4] C. Livermore, "Structures," 6.777J Lecture Notes, MIT, Spring, 2011 (unpublished)
- [5] Brotz J 2004 *Damping in CMOS-MEMS resonators* Master's thesis Carnegie Mellon University
- [6] D. Weinstein, "Damping," 6.777J Lecture Notes, MIT, Spring, 2011 (unpublished)
- [7] Jeon Y.R., Sood R., Kim S.G., "Piezoelectric Micro Power Generator for Energy Harvesting," *Sensors and Actuators A: Physical*, **122**, pp. 16-22, 2005.
- [8] Timoshenko S P and Goodier J 1970 *Theory of Elasticity* 3rd ed (McGraw Hill Higher Education)
- [9] Vip Sensors, premier supplier of sensors and sensor systems
<http://www.vipsensors.com/electronics/electronics.html>
- [10] Mide, commercial piezoelectric energy harvester provider <http://www.mide.com>